machines

MDPI

Article

Numerical and Experimental Characterization of a Railroad Switch Machine

Dario Croccolo, Massimiliano De Agostinis, Stefano Fini *, Giorgio Olmi and Francesco Robusto

Department of Industrial Engineering, University of Bologna, Viale del Risorgimento 2, 40136 Bologna, Italy; dario.croccolo@unibo.it (D.C.); m.deagostinis@unibo.it (M.D.A.); giorgio.olmi@unibo.it (G.O.); francesco.robusto2@unibo.it (F.R.)

* Correspondence: stefano.fini@unibo.it; Tel.: +39-051-2093455

Abstract: This contribution deals with the numerical and experimental characterization of the structural behavior of a railroad switch machine. Railroad switch machines must meet a number of safety-related conditions such as, for instance, exhibiting the appropriate resistance against any undesired movements of the points due to the extreme forces exerted by a passing train. This occurrence can produce very high stress on the components, which has to be predicted by designers. In order to assist them in the development of new machines and in defining what the critical components are, FEA models have been built and stresses have been calculated on the internal components of the switch machine. The results have been validated by means of an ad-hoc designed experimental apparatus, now installed at the facilities of the Department of Industrial Engineering of the University of Bologna. This apparatus is particularly novel and original, as no Standards are available that provide recommendations for its design, and no previous studies have dealt with the development of similar rigs. Moreover, it has wide potential applications for lab tests aimed at assessing the safety of railroad switch machines and the fulfilment of the specifications by many railway companies.

1. Introduction

A railroad switch machine (RSM), turnout or set of points is a mechanical installation enabling railway trains to be guided from one track to another, such as at a railway junction or where a spur or siding branches off. One of the key safety requirements of railroad switches is related to achieving a suitable resistance against any undesired movements of the points, due, for instance, to the extreme forces exerted by a passing train in the case of the needle leaned to the rail (force F in Figure 1).

Many railway companies assume a force F = 100 kN as standard. This work deals with the development of FEA models aimed at accomplishing the structural design of the RSM under the aforementioned operating load. In order to validate such models, an experimental test bench has been designed and manufactured. This comprises two ad-hoc designed fixtures that allow the accommodation of the test piece on a standard INSTRON 8500 500 kN standing press and the application of forces up to a maximum of F = 300 kN. Issues of novelty arise from the lack of studies both in the scientific and in the technical literature dealing with the development of similar fixture devices. The developed testing rig can be used not only for FEA validation purposes, but also for experimental tests aimed at warranting the safety of the RSM and the accomplishment of design requirements by most railway companies. The originality of the performed non-trivial design task arises also from the lack of specific Standards providing recommendations or reference schemes for the execution of lab tests aimed at assessing the structural response of RSM under high loads.
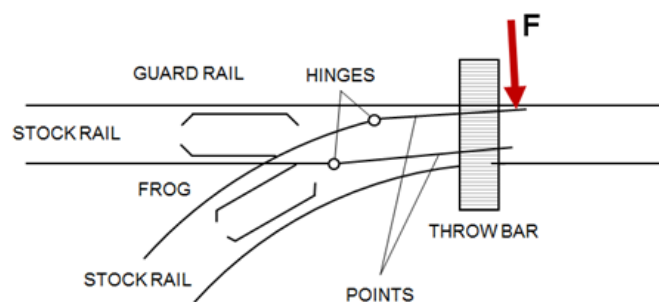
Figure 1. Geometry of a railroad switch.

2. Materials and Methods

The Alstom RSM object of the present investigation is shown in Figure 2, along with some balloons highlighting the key structural components of the machine.
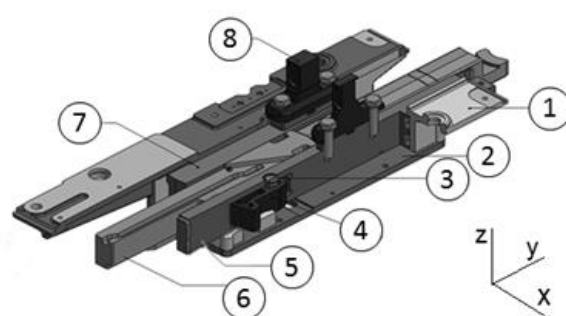

Figure 2. 3d model of the Alstom RSM: (**1**) body; (**2**) lower plate; (**3**) pin; (**4**) hammer; (**5**) switching rod; (**6**) cam; (**7**) detection rod; (**8**) arm.

Due to confidentiality-related issues, the working principles of the machine cannot be described in detail. The analysis was limited to the verification of the mechanism against unwanted movements of the points caused by a passing train since the system is equipped with two interlocking devices. In fact, once the full stroke has been travelled, and the points are in the open (or closed) position, the switching rod (5) is secured to the body (1) by means of a hammer (4); at the same time, the detection rod (7) is secured to the lower plate (2) by means of a slider, not represented in the picture. Therefore the locking devices come into effect preventing any movement of the rods, when an external force is applied along z-axis to the points, and thereby to the arms (8).

According to the requirements set by railway companies, the RSM should be validated under the action of a force F = 100 kN. The load application rate surely affects the response of the structure. The testing force of F = 100 kN is set by the railway company in order to account for dynamic effects. In order to attain an adequate stiffness of the test fixture, it has been dimensioned for a maximum load of 300 kN. The overall dimensions of the test piece are 900 × 300 × 210 mm; therefore, the fixture was conceived in two separate parts, a lower and an upper grip, so as to achieve a certain flexibility during mounting and unmounting operations on the standing press. In order not to transmit any unwanted bending moment at the arms, the test fixture was shaped as shown in Figure 3. While the lower grip is a simple C-shaped interface between the actuator thread and the arms, the upper grip has to retain the whole RSM by means of four M20 8.8 class bolts. The bolted joint is doubly overlapped: this provision allows doubling the frictional surfaces and hence the transmissible load for a given bolt size and class [1,2]. Except for a few details, the fixture has to be arc welded, therefore a structural steel S275JR according to [3] has been chosen for its construction. All the welds were statically dimensioned according to Standard EN 1993-1-8 [4]. In order to assess the stresses and the deformations on the fixture under maximum design load (F = 300 kN), some FEA have been performed by means of the commercial code Ansys Workbench.
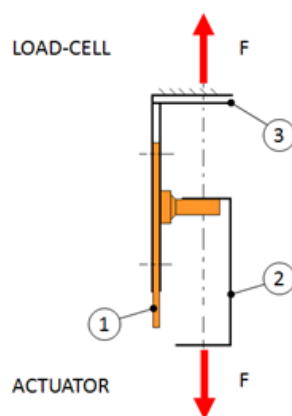
Figure 3. Loading scheme: (**1**) test piece (switch machine); (**2**) lower grip; (**3**) upper grip.

Figure 4a shows the boundary conditions applied to the model: the upper grip has been fixed at the upper end and loaded by two equal forces Fz = 150 kN, one at each arm. The model has been meshed with SOLID187 Tetrahedral and Hexahedral elements, Figure 4b. The material is a structural steel, whereas the bonded contacts are managed by means of the pure penalty contact algorithm, with the normal stiffness factor set to FKN = 0.01, following the lines suggested by [5,6]. The analysis and model parameters are summarized in Table 1.
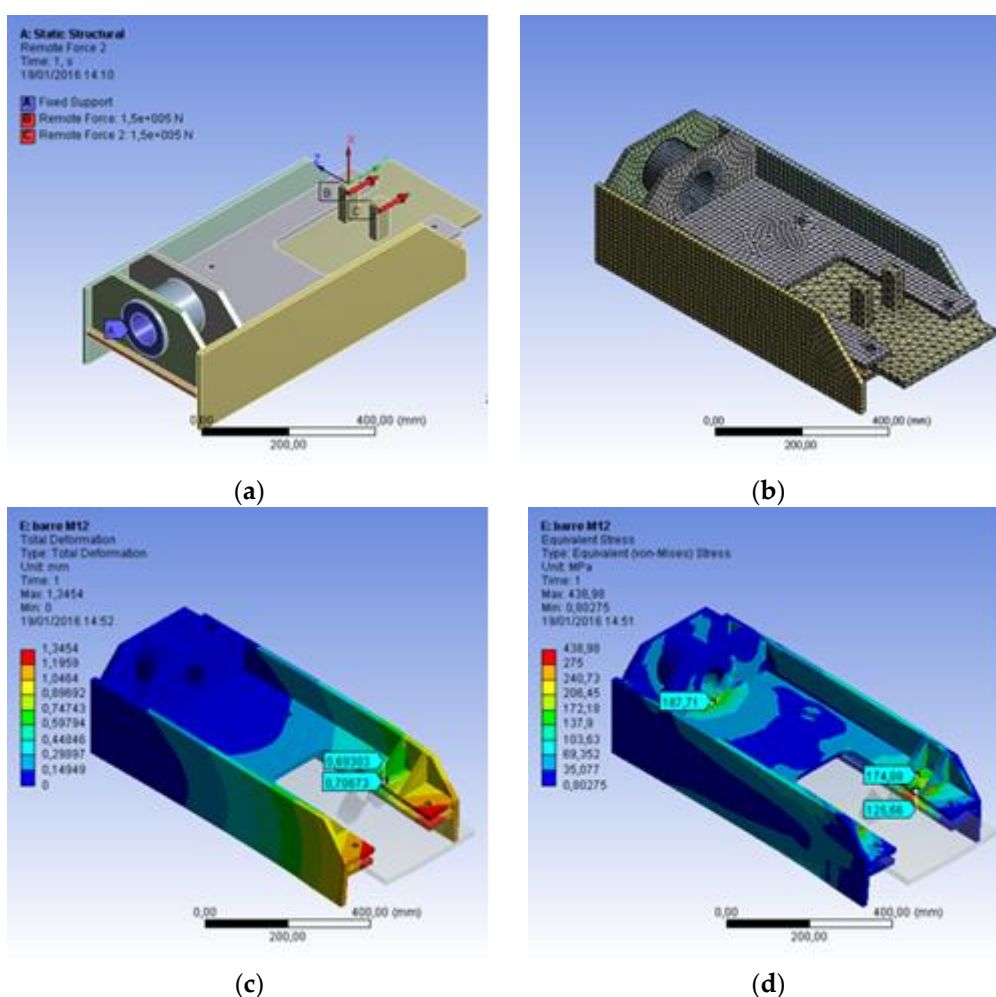

(**a**)

(**b**)

(**c**)

(**d**)

Figure 4. FEA on the fixture upper grip: (**a**) Boundary conditions; (**b**) mesh; (**c**) total deformation; (**d**) equivalent von Mises stress.

Table 1. Analysis and model parameters.

	Number of Nodes	Element Types	Elastic Modulus	Poisson Ratio
	[-]	[-]	E [Mpa]	ν [-]
Fixture	80,000	SOLID187 (Tetrahedral and Hexahedral)	200,000	0.3

As can be appreciated by looking at Figure 4c, the total deformation is Δtot_max = 1.3 mm, whereas the maximum von Mises equivalent stress remains below 190 MPa (see Figure 4d); such a stress level is well below the material yield point SY = 275 MPa. Since the model is linear, a maximum deformation of about Δtot_nom = 0.4 mm can be expected at nominal load, which is deemed acceptable.

The assembly procedure of the test rig requires quite a number of subsequent operations, briefly summarized in Figure 5. In particular, Figure 5d shows a detailed view of the arms of the machine when these are clamped by the lower grip. When the assembly is done, the load cell undergoes zero calibration and the test can begin. The main goal of the experiment is to provide a validation of the FEA models of the RSM that will be described in the following. A secondary aim of the experimentation is to determine how much of the total load is borne by the switching rod and how much by the detection rod. In order to accomplish this twofold task, three components of the RSM were instrumented by strain gauges: the two arms and the pin (see Figure 6).
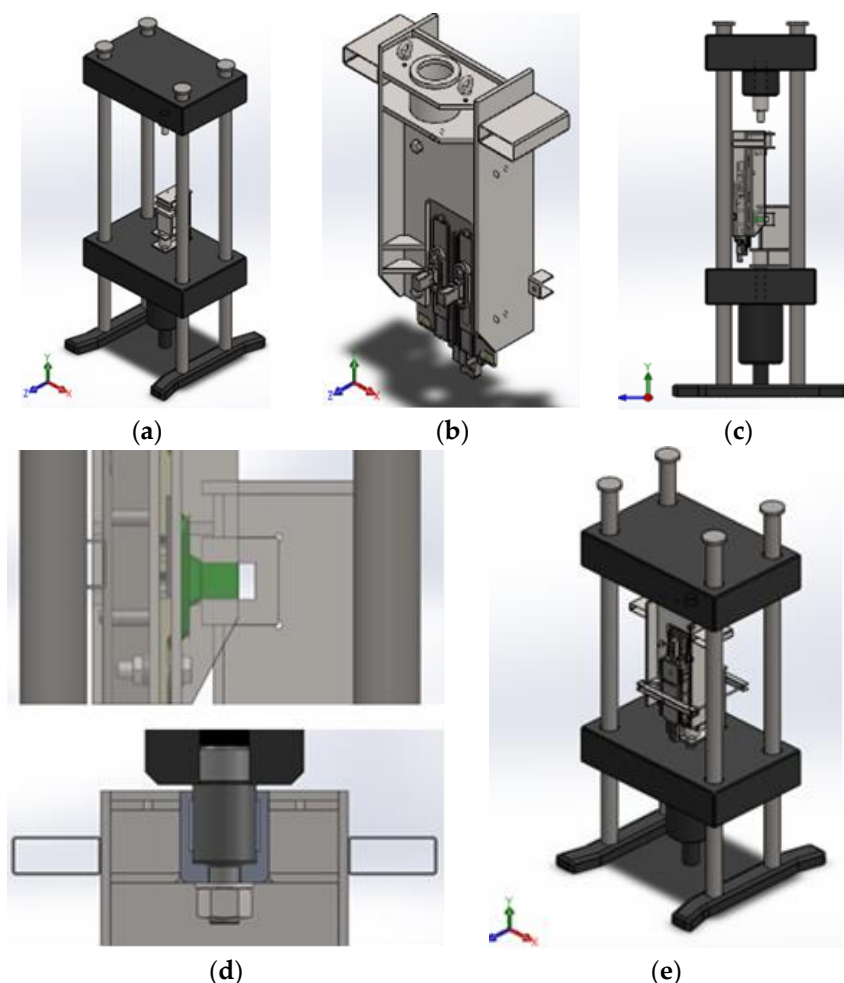

(a)   (b)   (c)

(d)   (e)

Figure 5. Test arrangement: (**a**) Placement of the lower grip, (**b**) pre-mounting of the upper grip with the test piece; (**c**) placement of the upper grip with a forklift; (**d**) details of the assembly; (**e**) final configuration.
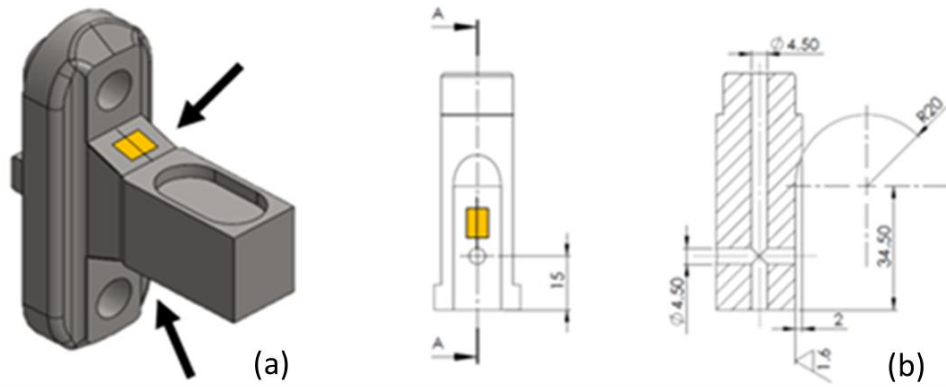
Figure 6. (**a**) Placement of the strain gauges on the arm and (**b**) on the reworked pin.

The pin and arms had been previously reworked in order to accommodate the sensors (Vishay Precision Group J2A-XXS047K-350); in particular, the pin required both milling and boring operations in order to achieve a plane surface for the application of the strain gauge, as well as a passage for the cables. The arms were instrumented by means of two strain gauges each; the strain gauges were connected in a half-bridge fashion to the Wheatstone circuit. The pin was instrumented by means of a single strain gauge; a dummy gauge, which served as a temperature drift compensator, was glued to an identical, unloaded pin placed in the testing room. The adhesive used for the installation was the M-BOND 200 by Vishay Precision Group. All the sensors were installed by a certified operator, following the guidelines suggested by the Standards [7–9]. Data acquisition was managed by means of the NI 9237 sampling card plugged into a NI cDAQ-9184 carrier. The FEA model of the RSM was developed by means of the Ansys code V.17. Due to the complexity of the assembly, submodeling was leveraged, by considering half a model at a time, as if the machine were cut along its mid-plane, normal to the *x*-axis. In this way, it was possible to find a satisfactory balance between accuracy and computational cost. Both models were meshed with tetrahedral elements SOLID187, switching rod side (Figure 7), and detection rod side (Figure 8). The analysis and model parameters are summarized in Table 2.
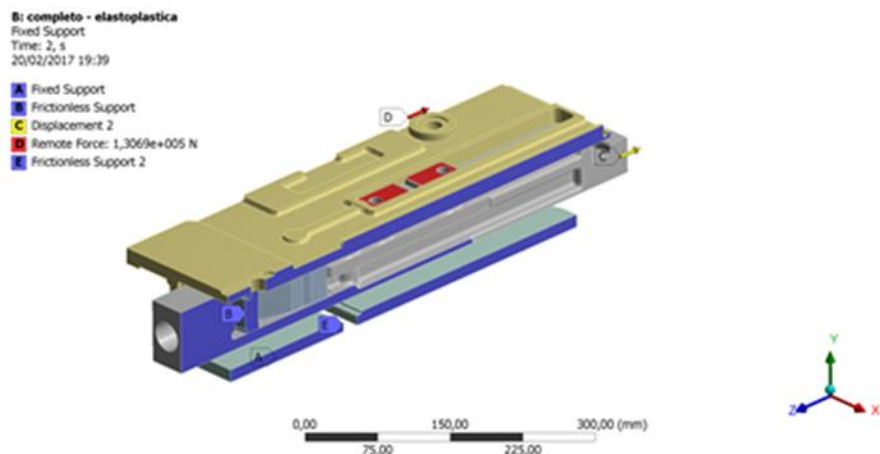

Figure 7. Boundary conditions for the half model comprising the switching rod.

Figure 8. Boundary conditions for the half model comprising the detection rod.

Table 2. Analysis and model parameters.

	Number of Nodes	Element Types	Steel Components		Cast Iron Components	
			Elastic Modulus	Poison Ratio	Elastic Modulus	Poisson Ratio
	[-]	[-]	E [Mpa]	ν [-]	E [Mpa]	ν [-]
RSM switching rod side	360,000	SOLID187 (Tetrahedral and Hexahedral)	200,000	0.3	169,000	0.275
RSM detection rod side	485,000	SOLID187 (Tetrahedral and Hexahedral)	200,000	0.3	169,000	0.275

In the case of the switching rod, the stresses on the pin and those on the hammer were sampled, and subsequently compared with the experimental outcomes. In the case of the detection rod, the stresses on the pins that connect the lower plate to the body were examined, as a function of the actual bolt preload of the joint.

3. Results and Discussion

The results from a tensile test carried out on the ad-hoc developed test bench are shown in Figure 9.
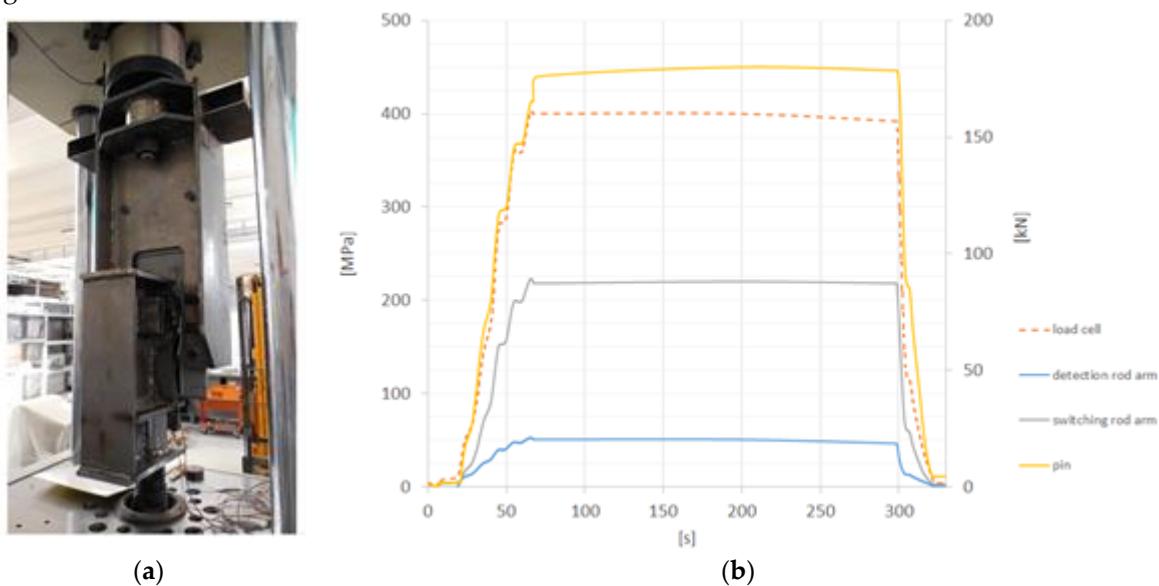

(**a**)   (**b**)

Figure 9. (**a**) View of the test bench and (**b**) plot of the results in terms of stresses on the pin and on the arms and force at the load cell.

Figure 9 reports the data relevant to a test run until a maximum force of F = 160 kN. At the peak load, one of the pins connecting the lower plate with the body failed. The first outcome of the

experiment is the knowledge of the force distribution on the two arms: the great majority of the total force (82%) reaches the body by passing through the chain of components named the switching rod, the pin and the hammer. The remaining part (18%) passes through the detection rod, the slider and the lower plate, eventually reaching the body. Running each of the FEA models by applying the appropriate fraction of the total load to the arm under investigation, it was possible to validate the numerical results. For example, looking at Figure 10a, it is possible to observe the equivalent stresses calculated according to the von Mises criterion on the half machine comprising the switching rod. Figure 10b reports the σY bending stresses on the pin that supports the hammer, when this sub-system is loaded with 82% the total load F = 160 kN.
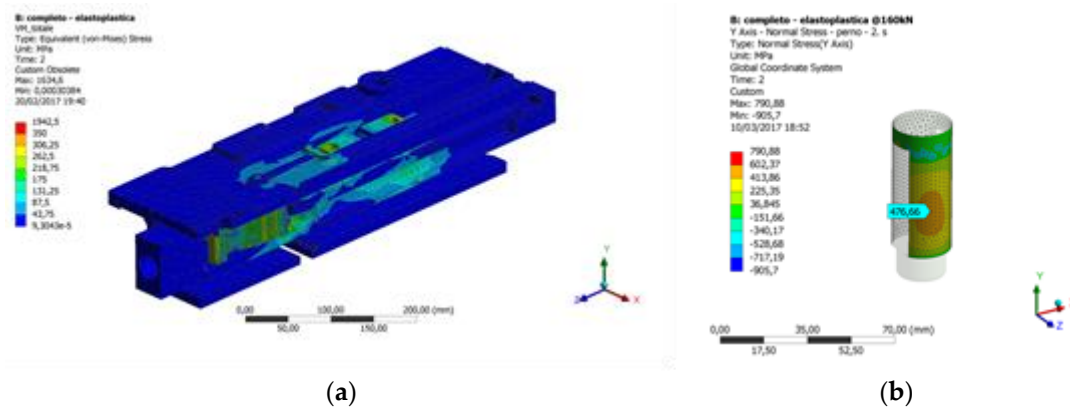

(**a**)   (**b**)

Figure 10. (**a**) von Mises stress plot on the half machine—switching rod side, and (**b**) bending σY stresses on the pin.

As can be appreciated from Figure 10b, the numerical peak of the bending stress on the pin (σY_FEA = 477 MPa) is very close to that measured during the experimental test on the same component (σY_EXP = 450 MPa, see Figure 9). The error, calculated according to Equation (1), is acceptable.

$$e\% = \frac{\sigma_{Y\_FEA} - \sigma_{Y\_EXP}}{\sigma_{Y\_EXP}} \cdot 100 = 6\% \tag{1}$$

Once the FEA model has been validated, it can be used for carrying out some comparisons considering, for example, the joint between the lower plate and the body. Such joints comprise a pattern of eight M8 8.8. screws, working in parallel with a couple of parallel pins of d = 6 mm diameter, manufactured according to Standard [10]. It can be assumed that this joint must withstand the shearing load transmitted by the slider to the body via the lower plate. These pins are coupled with interference (H7/m6). Since the screws are tightened under preload control upon assembly, and some uncertainties with regard to the friction coefficients cannot be avoided [11,12], the load borne by the parallel pins may vary depending on the effective preload of the screws and on the friction coefficient at the interface between the body and the plate. In order to estimate such variation, some parametric analyses were run, for example by imposing different preload levels on the screws. The screw preload was assigned via the preload tool available in the Ansys Workbench environment. Figure 11 reports a plot of the amount of shearing force borne by the switching rod side pin (T'swi) and by the detection rod side pin (T'det) as functions of the actual screw preload Fv. Each of the dashed lines represents the force acting on the relevant parallel pin, whereas the solid lines represent the fraction of load borne by the generic pin.
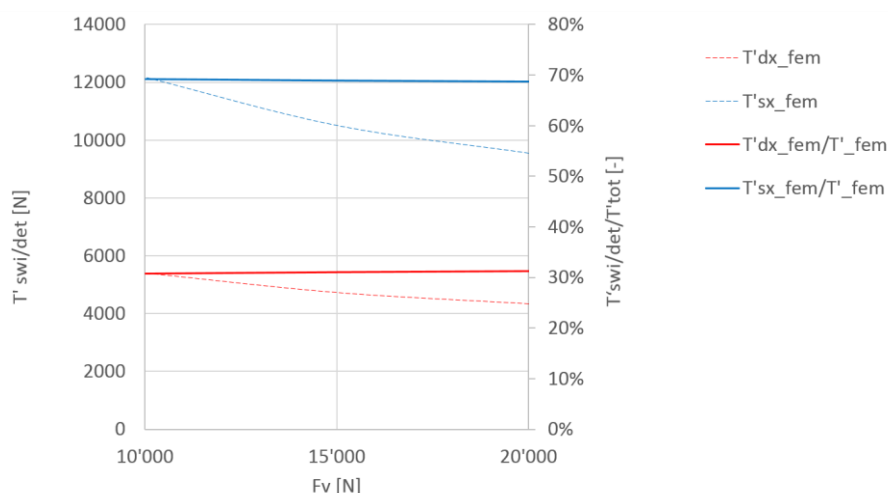
Figure 11. Shearing force on the switching/detection rod side parallel pin versus screw preload.

It can be seen that the most loaded pin is that on the detection rod side (closer to the slider), regardless of the screw preload. Nonetheless, the magnitude of the load borne by the pins decreases as the screw preload increases: a preload limit of Fv = 20 kN is assumed based on the provisions of Standard [13] for M8, 8.8 class screws. Based on different preload levels, it is also possible to extract a plot of the von Mises stresses on the most loaded parallel pin, as shown in Figure 12.
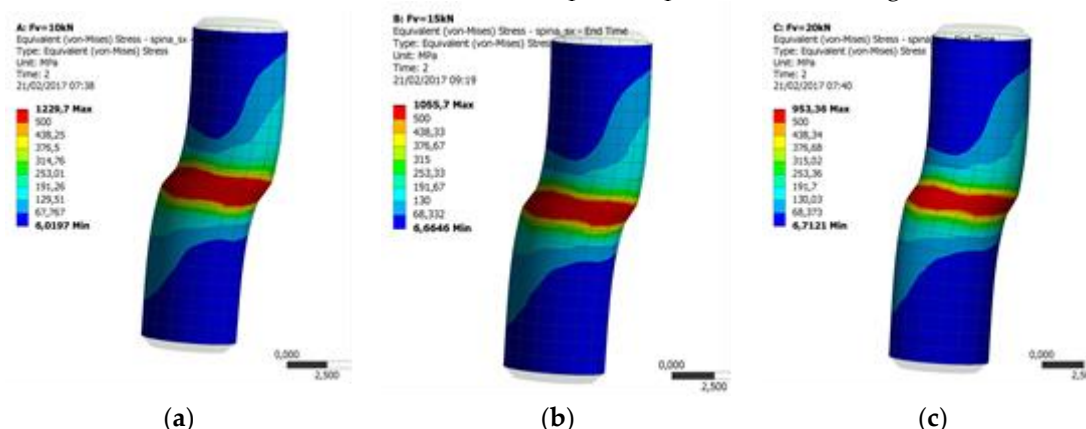

| (a) | (b) | (c) |

Figure 12. von Mises stress plot on the detection rod side parallel pin at a screw preload of (**a**) 10 kN; (**b**) 15 kN; (**c**) 20 kN.

The equivalent stress calculated by FEA on the most loaded parallel pin is compatible with the failure event, which took place during the experiment at a total load of F = 160 kN. The strength of the pins could be modified by changing the coupling system, increasing the interference or adopting a different coupling technique. Based on the literature, a valid alternative could be making use of anaerobic or epoxy adhesives, which would make it possible to significantly increase the actual mating area with a positive outcome in terms of the overall strength. This point has been tackled experimentally in papers [14–16], which also provide tips regarding the proportioning of the joint upon its design.

4. Conclusions

From a designer's standpoint, the present work achieved a twofold result: (i) an experimental setup has been designed, manufactured and calibrated, which is novel and original and will be useful for subsequent experimentations on other products of the same family; (ii) numerical tools have been developed and validated, with respect to experimental data. These models allow the designer to evaluate the effect of structural changes early, hence reducing the time to market of new machines.

References

1. Niemann, G.; Winter, H.; Hohn, B.R. *Maschinenelemente: Band 1: Konstruktion und Berechnung von Verbindungen, Lagern, Wellen*; Springer-Verlag: Berlin, Germany, 2005.
2. De Agostinis, M.; Fini, S.; Olmi, G. The influence of lubrication on the frictional characteristics of threaded joints for planetary gearboxes. *Proc. Inst. Mech. Eng. Part C: J. Mech. Eng. Sci.* **2016**, *230*, 2553–2563.
3. *Hot Rolled Products of Structural Steels, Part 2: Technical Delivery Conditions for Non-Alloy Structural Steels*; UNI EN 10025-2:2005; British Standards Institution: London, UK, 2005.
4. *Eurocode 3, Design of Steel Structures, Part 1-8: Design of Joints*; UNI EN 1993-1-8:2005; Europian Comittee for Standardisation: Brussels, Belgium, 2005.
5. Croccolo, D.; De Agostinis, M.; Vincenzi, N. Structural analysis of an articulated urban bus chassis via FEM: a methodology applied to a case study. *Strojniski Vestnik J. Mech. Eng.* **2011**, *57*, 799–809.
6. Zhao, X.; Li, F.; Fan, Y.; Liu, Y. Fatigue behavior of a box-type welded structure of hydraulic support used in coal mine. *Materials* **2015**, *8*, 6609–6622, doi:10.3390/ma8105325.
7. *Non Destructive Testing—Inspection by Strain Gauges: Terms and Definitions*; UNI EN 10478-1:1996; Italian Standards: Milano, Italy, 1996.
8. *Non Destructive Testing—Inspection by Strain Gauges: Selection of Strain Gauges and Accessory Components*; UNI EN 10478-2:1998; Italian Standards: Milano, Italy, 1996.
9. *Non Destructive Testing—Inspection by Strain Gauges: Strain Gauge Installation and Checking*; UNI EN 10478-3:1998; Italian Standards: Milano, Italy, 1998.
10. *Parallel Pins, of Hardened Steel and Martensitic Stainless Steel*; ISO 8734; International Organization for Standardization: Geneva, Switzerland, 1997. (Dowel pins)
11. Croccolo, D.; De Agostinis, M.; Fini, S.; Olmi, G. Tribological properties of bolts depending on different screw coatings and lubrications: An experimental study. *Tribol. Int.* **2017**, *107*, 199–205.
12. Eccles, W.; Sherrington, I.; Arnell, R.D. Frictional changes during repeated tightening of zinc plated threaded fasteners. *Tribol. Int.* **2010**, *43*, 700–707.
13. *Mechanical Properties of Fasteners Made of Carbon Steel and Alloy Steel—Part 1: Bolts, Screws and Studs with Specified Property Classes—Coarse Thread and Fine Pitch Thread*; ISO 898-1; International Organization for Standardization: Geneva, Switzerland, 2009.
14. Croccolo, D.; De Agostinis, M.; Mauri, P.; Olmi, G. Influence of the engagement ratio on the joint strength of press fitted and adhesively bonded specimens. *Int. J. Adhes. Adhes.* **2014**; *53*, 80–88.
15. Croccolo, D.; De Agostinis, M.; Fini, S.; Olmi, G. Influence of the engagement ratio on the shear strength of an epoxy adhesive by push-out tests on pin-and-collar joints: Part I: Campaign at room temperature. *Int. J. Adhes. Adhes.* **2016**, *67*, 69–75.
16. Croccolo, D.; De Agostinis, M.; Fini, S.; Olmi, G. Influence of the engagement ratio on the shear strength of an epoxy adhesive by push-out tests on pin-and-collar joints: Part II: Campaign at different temperature levels. *Int. J. Adhes. Adhes.* **2016**, *67*, 76–85.